Vortex Model Based Adaptive Flight Control Using Synthetic Jets

Jonathan A. Muse *
Georgia Institute of Technology, Atlanta, GA, 30332, USA
Andrew A. Tchieu †
California Institute of Technology, Pasadena, CA, 91125, USA
Ali T. Kutay‡, Rajeev Chandramohan *, and Anthony J. Calise §
Georgia Institute of Technology, Atlanta, GA, 30332, USA
and Anthony Leonard ¶
California Institute of Technology, Pasadena, CA, 91125, USA

A simple low-order model is derived for developing flight control laws for controlling the longitudinal dynamics of an aircraft using synthetic jet type actuators. Bi-directional changes in the pitching moment over a range of angles of attack are effected by controllable, nominally-symmetric trapped vorticity concentrations on both the suction and pressure surfaces near the trailing edge. Actuation is applied on both surfaces by hybrid actuators that are each comprised of a miniature obstruction integrated with a synthetic jet actuator to manipulate and regulate the vorticity concentrations. In previous work, a simple model was derived from a reduced order vortex model that includes one explicit nonlinear state for fluid variables and can be easily coupled to the rigid body dynamics of an aircraft. This paper further simplifies this model for control design. The control design is based on an output feedback adaptive control methodology that illustrates the effectiveness of using the model for achieving flight control at a higher bandwidth than achievable with typical static actuator assumptions. A unique feature of the control design is that the control variable is a pseudo-control based on regulating a *control vortex* strength. Wind tunnel experiments on a unique dynamics traverse verify that tracking performance is indeed better than control designs employing standard actuator modeling assumptions.

I. Introduction

The idea of using small, simple active flow control devices that directly affect the flow field over lifting surfaces sufficiently to create control forces and moments has attracted growing interest over the last decade. Compared to conventional control surfaces, flow control actuators have the potential benefits of reduced structural weight, lower power consumption, higher reliability, and faster output response. Significant work on open-loop flow control has already demonstrated control effectiveness on both static and rigidly moving test platforms. These studies have primarily focused on mitigation of partial or complete flow separation over stalled wing sections or flaps[1,2] . The lift and drag benefits associated with flow attachment enable control in a broader angle-of-attack range, however, these methods provide no direct control as they rely on conventional control surfaces for control actuation, and provide little benefit at moderate flight conditions. A different approach to flow control that emphasizes fluidic modification of the *apparent* aerodynamic shape of the surface by exploiting the interaction between arrays of surface-mounted synthetic jet actuators and

*Graduate Research Assistant, Aerospace Engineering, AIAA Student Member.
†Graduate Research Assistant, Graduate Aeronautical Laboratories, AIAA Student Member.
‡Research Engineer, School of Aerospace Engineering, Member
§Professor, School of Aerospace Engineering, AIAA Fellow
¶Professor Emeritus, Graduate Aeronautical Laboratories.

the local cross flow was recently developed[3,4] . With this approach bi-directional pitching moments can be induced by individually controlled miniature, hybrid surface actuators integrated with rectangular, high aspect ratio synthetic jets that are mounted on the pressure and suction surfaces near the trailing edge[5] . An important attribute of this technique is that it can be effective not only when the baseline flow is separated but also when it is fully attached, namely at low angles of attack such as at cruise conditions.

Despite the amount of the effort devoted to active flow control technology in recent years, a majority of the work published depends on experience and intuition rather than on a fundamental understanding of the flow physics. This is due to the lack of an analytical formulation of the mechanism behind flow actuation. Even though various aspects of flow actuation have been investigated experimentally, mostly on steady models, it is still difficult to draw conclusions and predict performance on dynamic models. This presents a challenge for feedback controller design as the vast majority of control synthesis techniques are inapplicable.

In our recent studies, we demonstrated successful closed-loop control of pitch motion of a 1-DOF and 2-DOF wind tunnel model by using the aforementioned actuators with no moving control surfaces[6,7] . First a linear controller was designed for the rigid body model of the test model by approximating the actuators as linear static devices. This controller worked well for slow maneuvers where the static actuator assumption holds. For faster maneuvers, requiring higher bandwidth controller design, interactions between the flow and vehicle dynamics get stronger and the linear rigid body model can no longer represent overall system behavior accurately. In these regimes, linear controllers that ignore effects of flow actuation have limited performance. A neural network (NN) based adaptive controller was introduced to improve the controller performance by compensating for the modeling errors in the design including the unmodeled dynamics of actuation. We assume that the system dynamics can be written as

$$\begin{aligned} \dot{x} &= Ax + B\left(u + \Delta\left(x, x_f, u\right)\right) \\ \dot{x}_f &= f\left(x, x_f, u\right) \end{aligned} \tag{1}$$

where x represents the rigid body states of the vehicle, x_f is the state vector associated with the dynamics of the flow, and $u = u_{dc} - u_{ad}$ is the control signal to the actuators with u_{dc} dc being the output of a linear dynamic compensator and u_{ad} the adaptive control signal. Matrices A and B form the linear system model used to design u_{dc} and Δ represents the modeling errors in rigid body dynamics and the couplings between the vehicle and unmodeled flow dynamics.

For slow maneuvers where changes in the flow field due to actuation occur much faster than the variations in the vehicle states, Δ remains comparatively small. In this case, the vehicle behavior approaches the linear design model and u_{dc} alone can control the system sufficiently well. As the vehicle starts moving faster, vehicle-flow interactions get stronger and Δ becomes large enough to disturb the vehicle's predictable dynamics. The adaptive controllers proposed[6,8] were shown on the experiment to successfully compensate for Δ for moderate bandwidths for a 1-DOF and a 2-DOF airfoil. The adaptive controller only used x and u feedback to compensate for Δ that is a function of x, u, and x_f. This is possible only if the x_f dependence of Δ is observable from x and u, which was evidently the case. For more aggressive maneuvers the observability assumption is likely to fail, or the dependence becomes much more complex. For such cases feedback from flow states is necessary to control the vehicle, which requires some information on $f(x, x_f, u)$ and $\Delta(x, x_f, u)$.

The objective of this research is to develop a low-order approximate flow model for the wind tunnel setup at Georgia Tech, validate it with the experiment data, and utilize it for simulation and control design. For our adaptive control design, a simple reduced order model is derived that captures the gross effect of the flow dynamics. The model is developed by simplifying a reduced order vortex model developed in our previous studies.[9] The reduced order vortex model includes only one explicit nonlinear state for fluid variables and can be easily coupled to the rigid body dynamics of an aircraft. The required modeling is mostly obtained from geometric information. The rest of the needed data is obtainable from simple static wind tunnel tests. A unique feature of control designs using this model is that the control variable is a pseudo-control based on regulating a *control vortex* strength. The control design is based on an output feedback adaptive control methodology that illustrates the effectiveness of using the model for achieving flight control at a higher bandwidth than achievable with a static actuator assumption. Since the linear model provides some information on f, this is incorporated into the linear part of the design (A and B

matrices in Eq. (1)), effectively reducing the amount of modeling error that the adaptive controller must compensate. This provides superior results compared to conventional modeling techniques. Experimental examples on a unique dynamic wind tunnel traverse verify that tracking performance is indeed better than control designs employing standard actuator modeling assumptions. The reduced order model from our previous work will also be used to simulate the system with higher accuracy. This is crucial to allow for investigation of various control architectures without spending expensive wind tunnel time.

II. Experimental Hardware

The experiments are conducted in an open-return low-speed wind tunnel having a square test section measuring $1m$ on the side. The present experiments use a 2-D airfoil model with a fixed cross section that is based on a NACA 4415 configuration as shown in figure 1. The chord length is $c = 457mm$, maximum thickness to chord ratio $t/c = 0.15$, and the model spans the entire width of the wind tunnel test section. The airfoil is modular and comprised of interchangeable spanwise segments which include a module of a circumferential array of 70 static pressure ports located at mid-span, and several modules of high-frequency integrated pressure sensors for measurements of instantaneous pressure. Bi-directional pitching moments induced by trapped vorticity flow-control are effected by individually-controlled miniature, hybrid surface actuators integrated with rectangular, high aspect ratio synthetic jets that are mounted on the pressure and suction surfaces near the trailing edge (Figure 1). The actuators have a characteristic height of 0.017c above the airfoil surface and the long dimension of the exit plane of each rectangular jet is parallel to the trailing edge and height (in the cross stream direction) of each jet orifice is 0.4 mm. The jets are generated by piezoelectric membranes that are built into a central cavity within the actuator and are operated off resonance within the range $1770Hz < f_{act} < 2350Hz$. The spanwise-segmented actuators are individually controlled from the laboratory computer and the system controller. The bulk of the present experiments are conducted at a free stream speed of $U_\infty = 30m/s$, with a corresponding Reynolds number based on the airfoil chord length of $Re_c = 8.55 \cdot 10^5$. At this speed, the actuation Strouhal number is $St = f_{act}c/U_\infty = 34$ and the maximum momentum coefficient is $C_\mu = 1 \cdot 10^{-3}$.

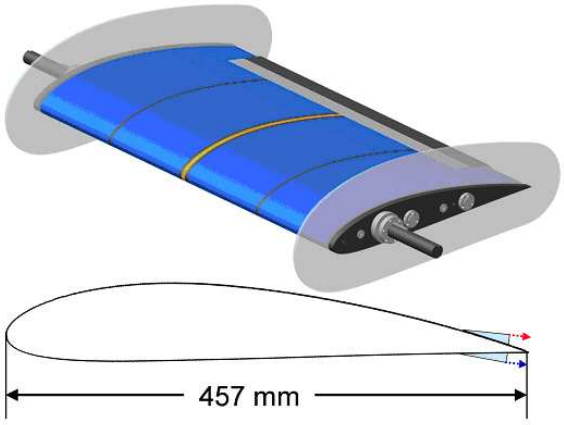

Figure 1. Render of wing model

In the present experiments, the wind tunnel model executes commanded flight maneuvers in two degrees of freedom (pitch and plunge) that are exclusively effected by flow control actuation within the constraints of the test section. The model is mounted on a programmable, 3-DOF (pitch, plunge, and roll) traverse that is constructed on an I-beam frame around the test section of the wind tunnel as shown in figure 2. The traverse is driven electromechanically by a dedicated feedback controller that removes the effect of parasitic mass and rotational inertia of the dynamic support system. The controller can also prescribe stability characteristics to mimic the behavior and control of a range of "virtual" air vehicles, all having the same wing as the wind tunnel model, but with static margins that can be adjusted by the traverse controller, including unstable configurations for high maneuverability.

The wing model is mounted on a rotating hollow shaft (which serves as conduit for wiring and pressure tubes). In one mode of operation pitch commands are executed by rotating the model using an AC servo

motor (torque motor) that is attached to one of the two vertical stages (figure 2) and is driven by a servo amplifier in torque mode to directly control the pitching moment on the model from the system's controller (the pitch range is limited to $\pm 25°$). At the opposite end the pitch shaft is supported by an air bearing that allows both rotational and axial motions. The axial motion allows the wind tunnel model to bank while it is maneuvered in pitch and plunge since the two plunge drives are controlled independently on each side of the tunnel. For open-outer-loop characterization the inner-loop controller is used to enforce a prescribed angle of attack $\alpha(t)$ trajectory. It also serves as a virtual variable tail surface by providing the torque required to trim the wing at any given condition, and by modifying its dynamic characteristics by changing its stiffness and damping properties. The application of torque $T(\alpha, \dot{\alpha}, \ddot{\alpha})$ effectively alters $\partial C_M/\partial\alpha$ and $\partial C_M/\partial\dot{\alpha}$ and the moment of inertia of the model, and allows for control of a range of stable and unstable configurations of "virtual" air vehicles. In addition, the servo motor is used as a transducer to indirectly measure the aerodynamic moment. In torque mode the motor generates a torque proportional to the input voltage and in steady state, the motor torque balances the aerodynamic moment, and moment due to gravity.

Vertical (plunge) commands are executed by two independently-controlled and synchronized linear slides mounted vertically on opposite sides of the wind tunnel test section. As shown in Figure 2, the linear slide on the left carries the pitch axis drive mechanism and the slide on the right carries the air bearing. Both ends of the pitch axis are connected to the linear slides through gimbals that allow free rotation about axes in the streamwise and cross stream directions, and prevent misalignment from binding the plunge slides. Each slide includes a carriage that is moved along rails by a $20mm$ pitch ball screw turned by an AC servo motor with an integrated encoder and an electromagnetic release brake that prevents load on the carriage when the traverse is not in operation. The travel of each linear slide is constrained by adjustable stops and limit switches. The model shaft moves in plunge through vertical slots in the side walls of the test section. The controller synchronizes the motion of the linear drives and thereby can enable controlled plunge and roll of the model. A force sensor based on a spring set and load cell system and linear accelerometers allow for measurements of the vertical forces and compensation for the weight and inertia of the model. In the present work, the linear motion of the model is software limited to speeds and accelerations of up to $0.5m/sec$ and $2g$, respectively (the maximum design speed and acceleration in the present configuration are $2.5m/sec$ and $5g$).

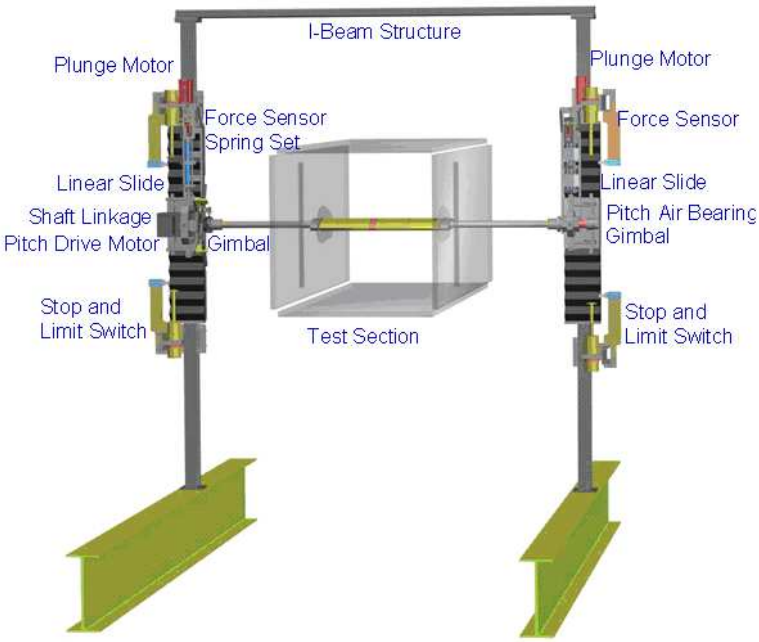

Figure 2. Render of traverse showing various components

III. Aerodynamic Model

A low-order vortex model for a pitching and plunging airfoil with trailing-edge synthetic jets was presented in Tchieu et. al. (2006)[9] . In this section we review that model for the purposes of developing a control design model. Unlike many other low or reduced-order models, this model is built from physical principles, i.e. the conservation of momentum. The vorticity in the model consists of freely-moving vortices in the wake, a trapped control vortex with circulation $\Gamma_C(t)$, and the boundary-layer vorticity on the airfoil surface. We consider small-amplitude motions of a flat-plate airfoil which leads to a number of simplifying assumptions. Thus, for example, all but one of the wake vortices move uniformly downstream along the nominal x-axis that is fixed to the airfoil. The exception is the vortex being fed circulation from the trailing edge. The velocity of the latter vortex is modified to conserve momentum as discussed below. In addition we assume that vorticity is shed into the wake to satisfy the unsteady Kutta condition (no velocity singularity) at the trailing edge. Also, a vortex sheet with a continuous distribution of vorticity $\gamma(x)$ is used to satisfy the boundary condition on the airfoil surface (normal component of velocity is continuous) plus the Kutta condition.

For the control input, the synthetic jet is modeled with a trapped vortex that represents the averaged effect of the actuation. The control vortex circulation depends on the control variable, u, for example,

$$\frac{d\Gamma_C}{dt} = F(u, \Gamma_C). \tag{2}$$

This function, F, can only be experimentally determined.

III.A. Wake Vortex Dynamics

Consider an airfoil of chord length c occupying the portion $-c/2 \le x \le c/2$ of the x-axis as presented in figure 3. The airfoil is undergoing small-amplitude motions in pitch and plunge. The pivot point for rotation is located at $x = -a$ as shown. The airfoil velocity is U in the negative x-direction. Alternatively, one could apply the results below to a stationary airfoil with a freestream velocity U in the positive x-direction. See figure 3 where the fluid flow and the airfoil motion are given relative to a frame of reference moving in the negative x-direction with the airfoil.

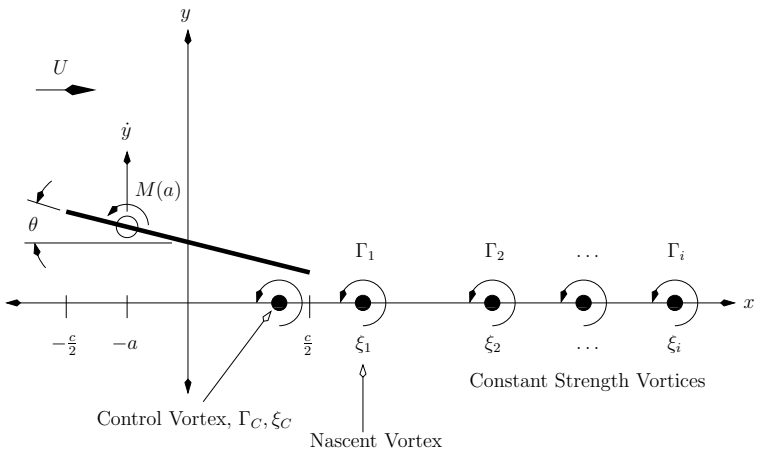

Figure 3. Pitching, plunging airfoil, control vortex with strength Γ_C, and free wake vortices with strengths $\Gamma_i, i = 1, ..., N$.

Now also consider a wake vortex with circulation Γ_i located at $x = \xi_i$. This vortex will result in a given distribution of vorticity on the airfoil, $\gamma_i(x)$, to satisfy the boundary condition on the airfoil and the Kutta condition given by (see, e.g., von Karman and Sears (1938)[10])

$$\gamma_i(x) = \frac{\Gamma_i}{\pi(\xi_i - x)} \sqrt{\frac{c/2 - x}{c/2 + x}} \sqrt{\frac{\xi_i + c/2}{\xi_i - c/2}}. \tag{3}$$

We find that

$$\int_{-c/2}^{c/2} \gamma_i(x)dx = \Gamma_i \left[\sqrt{\frac{\xi_i + c/2}{\xi_i - c/2}} - 1 \right]. \tag{4}$$

It appears that the correct location of the control vortex should be slightly forward of the trailing edge and just above the airfoil for suction-side actuation and just below the airfoil for pressure-side actuation. The total effect of both actuators can be represented by a single vortex on the mid-plane located slightly forward of the trailing edge. In any event, the control vortex with strength Γ_C will produce a corresponding contribution to the airfoil circulation given by $\gamma_C(x)$. We assume that a change in Γ_C on its own produces no net change of circulation in the wake. Thus,

$$\int_{-c/2}^{c/2} \gamma_C(x)dx = -\Gamma_C. \tag{5}$$

The total circulation, which must equal 0, is therefore given by

$$\Gamma_0 + \sum_{i=1}^{N} \Gamma_i \sqrt{\frac{\xi_i + c/2}{\xi_i - c/2}} = 0. \tag{6}$$

Here Γ_0 is the quasisteady circulation about the airfoil that depends only on the pitch angle, its time derivative, and the plunge rate, and N is the number of free vortices in the wake.

It is also assumed that all but one of the free vortices in the wake move with speed U. Thus,

$$\frac{d\xi_i}{dt} = U \quad (i \geq 2), \tag{7}$$

and the vortex being fed circulation (labeled $i = 1$) moves with speed

$$\frac{d\xi_1}{dt} = U - \frac{(\xi_1^2 - c^2/4)}{\xi_1 \Gamma_1} \frac{d\Gamma_1}{dt} \tag{8}$$

where we have used conservation of impulse to derive Eq. (8). This is in contrast with previous models where the force on the vortex and branch cut system was forced to be invariant.[11–14] It has been found that this so-called Brown-Michael correction introduces the incorrect initial lift curve for the specific case of the flat-plate undergoing an impulsive start. The conservation of impulse argument given above, correctly captures the initial behavior for this specific case.

Except for the vortex being fed, all vortices in the wake remain at constant circulation, i.e.

$$\frac{d\Gamma_i}{dt} = 0 \quad (i \geq 2). \tag{9}$$

The strength of Γ_1 is such that Eq. (6) remains satisfied. As mentioned earlier, the circulation of the control vortex is given, for example, by

$$\frac{d\Gamma_C}{dt} = F(u, \Gamma_C), \tag{10}$$

where u is the control variable and the function f is to be determined. With the absence of a model for Eq. (10), Eqs. (6)-(9) constitute a close system of equations for the wake dynamics of the system given a sufficient initial condition. Since Eqs. (7) and (9) are easily integrable, this system can be reduced to one non-linear differential, i.e. Eq. (8), with the algebraic constraint represented by Eq. (6). In accordance to Eq. (1), the fluid states are represented by $x_f = [\xi_1 \Gamma_1]^T$. In contrast to other models, the fluid state is directly related to the physical variables of vortex location and strength.

III.B. Lift and Moment Relationships

From the results derived in our previous work,[9] we have the following expressions for the lift and moment.

$$L = -\rho\pi(\frac{c^2}{4}\ddot{y} + Uc\dot{y}) - \rho\pi\left[\frac{ac^2}{4}\ddot{\theta} + U(a+\frac{c}{2})c\dot{\theta} + (\frac{\dot{U}c^2}{4} + U^2c)\theta\right] - \frac{\rho Uc}{2}\sum_{i=1}^{N}\frac{\Gamma_i}{\sqrt{\xi_i^2 - c^2/4}} - \rho U\Gamma_C, \quad (11)$$

and

$$M(a) = aL + \frac{\rho\pi Uc^2}{4}\dot{y} - \rho\pi\left[\frac{c^4}{128}\ddot{\theta} - \frac{Uac^2}{4}\dot{\theta} - \frac{U^2c^2}{4}\theta\right] + \frac{\rho Uc^2}{8}\sum_{i=1}^{N}\frac{\Gamma_i}{\sqrt{\xi_i^2 - c^2/4}} - \rho U\Gamma_C\xi_C, \quad (12)$$

The lift coefficient, defined as $C_L = 2L/(\rho Uc^2)$, is

$$C_L = -\pi(\frac{c}{2U^2}\ddot{y} + \frac{2}{U}\dot{y}) - \pi\left[\frac{ac}{2U^2}\ddot{\theta} + \frac{2a+c}{U}\dot{\theta} + \frac{c\dot{U} + 4U^2}{2U^2}\theta\right] - \frac{1}{U}\sum_{i=1}^{N}\frac{\Gamma_i}{\sqrt{\xi_i^2 - c^2/4}} - \frac{2}{Uc}\Gamma_C, \quad (13)$$

and the moment coefficient (with pitch up as positive) $C_M = -2M(a)/(\rho U^2c^2)$ is

$$C_M = \frac{a}{c}C_L + \frac{\pi}{2U}\dot{y} - \pi\left[\frac{c^2}{64U^2}\ddot{\theta} - \frac{a}{2U}\dot{\theta} - \frac{1}{2}\theta\right] + \frac{1}{4U}\sum_{i=1}^{N}\frac{\Gamma_i}{\sqrt{\xi_i^2 - c^2/4}} - \frac{2\xi_C}{Uc^2}\Gamma_C. \quad (14)$$

The above equations can quite be integrated in time easily. Equation 8 is singular when $t = 0$. In general, a small-time, asymptotic solution is necessary to provide a sufficient initial condition for the startup of the simulation. This model uses a different strategy to determine $\xi_1(t)$ and $\Gamma_1(t)$. From the conservation of total circulation, Eq. (6), we can write

$$\Gamma_1\sqrt{\frac{\xi_1 + c/2}{\xi_1 - c/2}} = -\Gamma_0 + \sum_{i=2}^{N}\Gamma_i\sqrt{\frac{\xi_i + c/2}{\xi_i - c/2}} \equiv G(t), \quad (15)$$

where the newly defined function $G(t)$ can be considered known up to time t. In addition, Eq. (8) can be written as

$$\frac{d}{dt}(\sqrt{\xi_1^2 - c^2/4}\,\Gamma_1) = \frac{\xi_1\Gamma_1 U}{\sqrt{\xi_1^2 - c^2/4}} = \frac{\xi_1 GU}{\xi_1 + c/2}. \quad (16)$$

Defining

$$H(t) \equiv \sqrt{\xi_1^2 - c^2/4}\,\Gamma_1, \quad (17)$$

we can write Eq. (16) as

$$\frac{dH}{dt} = \frac{H + cG/2}{H + cG}GU, \quad (18)$$

where we have used Eqs. (15) and (17) to determine ξ_1 as

$$\xi_1 = \frac{H + cG/2}{G}. \quad (19)$$

Similarly, Γ_1 is found to be

$$\Gamma_1 = G\sqrt{\frac{H}{H+cG}}. \tag{20}$$

WIth this approach, integrating equation (18) is numerically is now straightforward. Physically we expect that $\Gamma_1(t)$ cannot decrease in magnitude as time progresses. Let t^* be a time when $d\Gamma_1/dt$ changes sign. Thus we check, after each time increment, to see if Γ_1 has decreased in magnitude. If so, we return to the previous time t, which, by definition, $t = t^*$, and add the present Γ_1 and ξ_1 to the list of wake vortices labeled $i \geq 2$ and form a new $i = 1$ vortex with initial conditions $\xi_1(t^*) = c/2$ and $\Gamma_1(t^*) = 0$. Typically, near $t \approx t^*$ ($t > t^*$) we expect $G \sim t - t^*$ which leads to $\xi_1 \approx 1 + U(t-t^*)/4$ and $\Gamma_1 \approx G(t)\sqrt{U(t-t^*)/8}$ for $U(t-t^*) \ll 1$. An exception to this behavior would occur, for example, for an impulsive start at $t = 0$ with say $G(0) = -\Gamma_0(0) \neq 0$. In this case, $\xi_1 \approx 1 + Ut/2$ and $\Gamma_1 \approx -\Gamma_0(0)\sqrt{Ut/4}$ for $U(t-t^*) \ll 1$.

III.C. Rigid-Body Dynamics

Dealing with the fluid and body interaction problem is usually a difficult problem. For this case, due to the low-order fluid model, a closed system of equations can be constructed to predict the orientation and the motion of the airfoil. To model an airfoil is free flight it is assumed that the airfoil is attached to a spring and damper in the y-direction in addition to a torsional spring and damper in the θ-direction. This stabilizes the system and gives a model for non-stalled flutter in cross-flow.[15]

The system of equations for the airfoil in this configuration becomes

$$\begin{aligned} m\ddot{y} - S_x\ddot{\theta} + b_y\dot{y} + k_y y &= L \\ I\ddot{\theta} - S_x\ddot{y} + b_\theta\dot{\theta} + k_\theta y &= M(a) \end{aligned} \tag{21}$$

where L is the lift, $M(a)$ is the moment about the location a, S_x is the static imbalance per unit width, and all other terms are related to the linear and rotational mass, damping, and stiffness of the system.[b] The static imbalance per unit width is defined as

$$S_x \equiv \int \xi \rho_s d\xi d\eta$$

This is an area integral in a principle coordinate system where ρ_s is the density of the structure, and ξ and η are the principle coordinates. This can equivalently be expressed as

$$S_x = ma$$

where m is the mass of the object and a is the distance from the elastic axis (the point at which the springs and dampers are attached) to the center of mass, previously defined in figure 3.

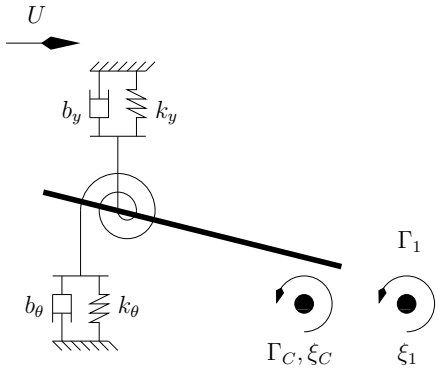

Figure 4. Schematic showing the configuration of rigid body coupling. Here the rigid body is attached to a mass-damper-spring system in both the plunge and pitching degrees of freedom. See figure 3 for more detail.

III.D. Non-zero Thickness and Camber Correction

This model assumes that the wing is a flat plate. To correct the neglected effect of thickness and camber on the lift and moment, we introduce corrections to the lift coefficient and moment coefficients in Eqs. (13) and (14). It is believed that the corrections are static and do not depend on the angle of attack in the range of operation or the unsteady maneuvering. Thus we simply add the the zero angle of attack lift and moment coefficient to obtain

$$\begin{aligned} \tilde{C}_L &= C_{L,0} + C_L \\ \tilde{C}_M &= C_{M,0} + C_M \end{aligned}$$

[b]Note that a right hand system has been used in this case, thus positive θ (or moment) corresponds to pitch down.

For example, on a clean NACA 4415 airfoil, the moment coefficient is nearly constant through the quarter chord for the range of angle of attacks in this study and thus $C_{M,0} \approx -0.1$.[16] For the lift coefficient, the change in lift per angle of attack for the NACA 4415 is nearly that of a flat plate and thus we correct the lift by offsetting the lift coefficient by the zero angle of attack lift for a NACA 4415, i.e. $C_{L,0} \approx 0.4$. Of course, this correction is wing section dependent and is taken from experimental results. This results in the following lift and moment corrections.

$$\tilde{L} = L + \left(\frac{1}{2}\rho U^2 c\right) C_{L,0}$$
$$\tilde{M} = M - \left(\frac{1}{2}\rho U^2 c^2\right) C_{M,0} + \left(a - \frac{c}{4}\right)\left(\frac{1}{2}\rho U^2 c\right) C_{L,0}$$

In our experiments, the c.g. is close to quarter chord and M simplifies since $\left(a - \frac{c}{4}\right) \approx 0$.

IV. Control Formulation

Though the developed model is a set of ordinary differential equations, it cannot be used for control design. Due to the highly nonlinear manner in which a vortex is added, the model is not casual. If the error caused by not resetting the time step in the model is neglected, the model can be made casual. However, because a vortex is created at each time the nascent vortex strength changes sign, at which point, the model resets the fluid dynamic states, i.e. it resets the location of the vortex at $\xi_c = c/2$ and the corresponding strength to $\Gamma_C = 0$. This is a result of the low-order nature of the model. While in this model the number of model states are kept fixed, in reality the number of vortices ultimately increases. To circumvent this problem the previous states are reused for the newest vortex. This causes a discontinuity in both the vortex position and strength when a new vortex is shed.

IV.A. A Simplified Control Design Model

The vortex model by its nature captures some dynamics that negligible on the time scales of a flight control system. From this prospective, it is reasonable to expect that it is possible to simplify the model further to make it appropriate for control design. When examining the lift and moment equations, (11) and (12), we observe that it is a function of only the states of the rigid body (i.e. both the added mass and the quasi-steady terms) in addition to a term due to the wake. For example, consider the lift equation. In this case, the term due to the wake is simply

$$L_W = -\frac{\rho U c}{2} \sum_{i=1}^{N} \frac{\Gamma_i}{\sqrt{\xi_i^2 - c^2/4}} \tag{22}$$

Therefore, we define a characteristic circulation for the entire wake as

$$\Gamma_W = c \sum_{i=1}^{N} \frac{\Gamma_i}{\sqrt{\xi_i^2 - c^2/4}} \tag{23}$$

Even though the discontinuities of the flow (i.e. the startup of Γ_i and ξ_i) are included in this term, Γ_W is fairly smooth. Hence, its reasonable to model this term using an ordinary differential equation. To choose a satisfactory differential equation, examine the startup case where $d\Gamma_w/dt = 0$ and only a single vortex is created. In this case

$$L = -\rho U \left(\Gamma_0 + \frac{1}{2}\Gamma_W\right) \tag{24}$$

From classical theory, it is expected that half of the lift is attained at the moment the plate is impulsively started from rest. Thus, at $t = t_0$, $\Gamma_W \approx -\Gamma_0$. When $t \to \infty$, the lift term due to the wake term should disappear as the wake vortices move further and further away. Therefore we propose using the model

$$\frac{d\Gamma_W}{dt} = -\frac{d\Gamma_0}{dt} - \beta\Gamma_W \tag{25}$$

where β is a constant.

Note that this introduces an exponential decay of Γ_W (which gives a $1-e^{\beta t}$ rise in lift) given a constant Γ_0. This is contrary to the classical square root type growth for the lift and a decay in the lift that is geometric at best. We choose β to best fit the case of an impulsive start flat plate by computing a norm between the original model and the simple model. The best fit for a given $\Delta t = T$ is given in table 1. We chose $\beta = 0.406$.

T	β
20	0.333
10	0.360
5	0.406

Table 1. Best fit for β

From this, a linear model can be formed consisting of geometrical parameters and the derivatives of y and θ. The differential equation governing the fluid dynamics reduces to a simple first order differential equation

$$\dot{\Gamma}_W + \beta\Gamma_W = -\pi c\left(\ddot{y} + \left(a + \frac{c}{4}\right)\ddot{\theta} + U\dot{\theta}\right) \tag{26}$$

with an initial condition of

$$\Gamma_W(t_0) = -\pi c\left[\dot{y} + \left(a + \frac{c}{4}\right)\dot{\theta} + U\theta\right]_{t=t_0} \tag{27}$$

Furthermore, the lift and moment expressions simplify to:

$$L = -\rho\pi\left(\frac{c^2}{4}\ddot{y} + Uc\dot{y}\right) - \rho\pi\left[\frac{ac^2}{4}\ddot{\theta} + U\left(a + \frac{c}{2}\right)c\dot{\theta} + \left(\frac{\dot{U}c^2}{4} + U^2c\right)\theta\right] - \frac{\rho U}{2}\Gamma_W - \rho U\Gamma_C \tag{28}$$

and

$$M = aL + \frac{\rho\pi U c^2}{4}\dot{y} - \rho\pi\left[\frac{ac^2}{128}\ddot{\theta} - \frac{Uac^2}{4}\dot{\theta} - \frac{U^2c^2}{4}\theta\right] + \frac{\rho Uc}{8}\Gamma_W - \rho U\Gamma_C\xi_C \tag{29}$$

The above equations include added mass, quasi-steady lift, lift due to wake, and control terms.

V. Linear Control Formulation

For control design is desirable to rewrite the simplified equations of motion as a matrix quadruple. To this end, we can equate equations (28), (29), and (21) to form the rigid body differential equations as

$$M\begin{bmatrix}\ddot{y}\\ \ddot{\theta}\end{bmatrix} + D\begin{bmatrix}\dot{y}\\ \dot{\theta}\end{bmatrix} + K\begin{bmatrix}y\\ \theta\end{bmatrix} + A\Gamma_w = B\Gamma_c \tag{30}$$

where the mass matrix M is given by

$$M = \begin{bmatrix} m + \frac{\rho\pi c^2}{4} & -S_x + \rho\pi\frac{ac^2}{4} \\ -S_x + \frac{a\rho\pi c^2}{4} & I + a\rho\pi\frac{ac^2}{4} + \rho\pi\frac{c^4}{128}\end{bmatrix} \tag{31}$$

the stiffness matrix is given by

$$K = \begin{bmatrix} k_y & \rho\left(\frac{\dot{U}c^2}{4} + U^2c\right) \\ 0 & k_\theta - \rho\pi\left(\frac{U^2c^2}{4} - \frac{a\dot{U}c^2}{4} - aU^2c\right)\end{bmatrix} \tag{32}$$

the damping matrix is given by

$$D = \begin{bmatrix} b_y + \rho\pi Uc & \rho\pi U\left(a + \frac{c}{2}\right)c \\ \rho\pi c\left(aU - \frac{Uc}{4}\right) & b_\theta + a\rho\pi U\left(a + \frac{c}{4}\right)\end{bmatrix} \tag{33}$$

and the aerodynamics coupling matrix, A, and the control matrix, B, is given by

$$A = \begin{bmatrix} \frac{\rho U}{2} \\ \rho U\left(\frac{a}{2} - \frac{c}{8}\right) \end{bmatrix}, \quad B = \begin{bmatrix} -\rho U \\ -\rho U\left(\xi_c + a\right) \end{bmatrix} \tag{34}$$

The governing relation for aerodynamics in equation (26) combined with (30) is used to form the required matrix quadruple

$$\begin{aligned} \dot{\bar{x}} &= \bar{A}\bar{x} + \bar{B}\Gamma_c \\ y &= \bar{C}\bar{x} + \bar{D}\Gamma_c \end{aligned} \tag{35}$$

where the system state, $\bar{x} = [y \;\; \theta \;\; \dot{y} \;\; \dot{\theta} \;\; \Gamma_w]^T$ and

$$\bar{A} = \begin{bmatrix} 0 & I & 0 \\ -M^{-1}K & -M^{-1}D & -M^{-1}A \\ \pi c\left[1 + \left(a + \frac{c}{4}\right)\right] M^{-1}K & \pi c\left[1 + \left(a + \frac{c}{4}\right)\right] M^{-1}D - \begin{bmatrix} 0 & \pi c U \end{bmatrix} & \pi c\left[1 + \left(a + \frac{c}{4}\right)\right] M^{-1}A - \beta \end{bmatrix} \tag{36}$$

and

$$\bar{B} = \begin{bmatrix} 0 \\ M^{-1}B \\ -\pi c\left[1 + \left(a + \frac{c}{4}\right)\right] M^{-1}B \end{bmatrix}, \quad \bar{C} = \begin{bmatrix} 1 & 0 & 0 & 0 & 0 \\ 0 & 1 & 0 & 0 & 0 \\ 0 & 0 & 1 & 0 & 0 \\ 0 & 0 & 0 & 1 & 0 \end{bmatrix}, \quad D = \begin{bmatrix} 0 \\ 0 \\ 0 \\ 0 \end{bmatrix} \tag{37}$$

Note that the control term Γ_C is a non-physical variable that is related to control voltage and the system states. This relationship will be explored in more detail later in the paper. Also, not all of the states are measurable. If all of the states were measurable, it is easy to formulate a control design based on LQR theory. In this paper, the nominal control design consists of a robust servomechanism LQR control law with augmented feed forward term to improve transient error tracking response. Consider the linear time invariant state space model:

$$\begin{aligned} \dot{x} &= Fx + Gu + Ew \\ y &= Hx \end{aligned} \tag{38}$$

where $x \epsilon \mathcal{R}^n$, $u \epsilon \mathcal{R}^m$, $w \epsilon \mathcal{R}^m$ and $y \epsilon \mathcal{R}^l$. Furthermore, it is assumed that w is an unmeasurable disturbance. Next we define the command input vector $r \epsilon \mathcal{R}^p$ such that r satisfies the differential equation given in 39 and we assume that the disturbance w satisfies the same differential equation.

$$r^{(p)} = \sum_{i=1}^{p} a_i r^{(p-i)} \tag{39}$$

Assuming that the $p < l$ and defining the error signal as:

$$e = y - r \tag{40}$$

and given the control objective that the command error $e(t) \to 0$ as $t \to \infty$ in the presence of unmeasured disturbances satisfying 39, it is possible design an optimal stabilizing control law for the plant dynamics given in 38. The solution of this standard formulation is derived in Wise[17] and yields that nominal control signal of the form:

$$u = -K_e \int_0^t e(\tau) d\tau - K_x x \tag{41}$$

Letting r satisfy $\dot{r} = 0$, the LQR based technique yields an integral action on the tracking error that allows for robust tracking of commands with zero steady state error. Augmenting the control law in 41 with

a feedforward term, Z, and allowing for an additional augmenting control input, Δu, for adaptive control design the final nominal control law is given by:

$$u = -K_e \int_0^t e(\tau)d\tau - K_x x + Zr + \Delta u \tag{42}$$

Graphically this can be represented as the simulation diagram shown in figure 5. The effect of the feedforward term is to help speed up the transient response of the control law. From a frequency domain standpoint, the eigenvalues of the closed loop system remain fixed under a constant gain Z. In a SISO system, this is equivalent to adding an adjustable zero that allows the designer to cancel a slow pole in closed loop transfer function $\frac{Y(s)}{R(s)}$.

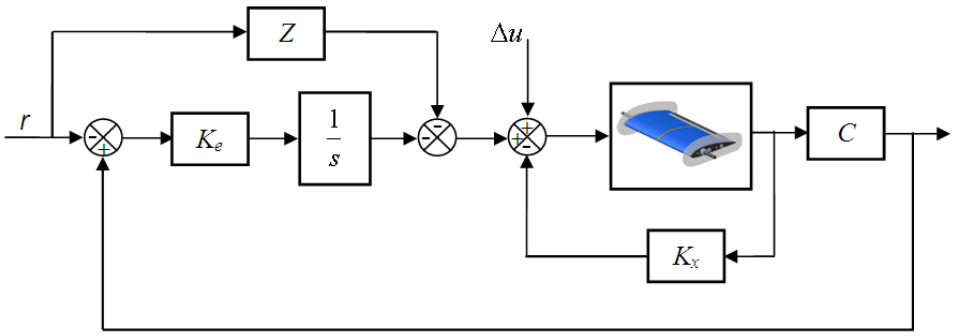

Figure 5. Robust Servo LQR with feedforward element and added control signal

Since the system is not full state feedback, we use the static projective control technique[17] , to formulate an output feedback law without feedback of the flow state. Augmenting the model dynamics with the control law dynamics, the closed loop system is given by

$$\begin{bmatrix} e \\ \dot{x} \end{bmatrix} = \begin{bmatrix} 0 & C_t \\ -\bar{B}K_e & \bar{A} - \bar{B}K_X \end{bmatrix} \begin{bmatrix} \int e \\ x \end{bmatrix} + \begin{bmatrix} -1 \\ \bar{B}Z \end{bmatrix} r$$

$$y_t = \begin{bmatrix} 0 & C_t \end{bmatrix} \begin{bmatrix} e \\ x \end{bmatrix}$$

where C_t is a matrix that multiplied by x that gives the plunge position, z. Since, we are not using the flow state in feedback we can retain all but two of the closed loop eigenvalues. Let $K = [K_e \quad K_x]$ and X_y be the eigenvectors corresponding to the closed loop eigenvalues we wish to retain. Then the required output feedback gain is computed as

$$\bar{K} = KX_y \left(\bar{C}_{meas} X_y\right)^{-1}$$

where $\bar{C}_{meas}$ corresponds to measured states of x such that $y_{meas} = \bar{C}_{meas} x = [\int e \quad y \quad \theta \quad \dot{y} \quad \dot{\theta}]^T$. The projective control effort is then defined by

$$\Gamma_C = -\bar{K} \begin{bmatrix} \int e \\ y_{measured} \end{bmatrix} + Zr$$

Though this technique does not guarantee closed loop stability, in practice, closed loop stability is easily satisfied.

V.A. Augmenting Output Feedback Adaptive Control

The assumed linear dynamics of the model (35) ignores nonlinearities and unmodeled dynamics associated with the flow actuation process. We assume that the true dynamics of the system can be represented as:

$$\begin{aligned} \dot{x} &= \bar{A}x + \bar{B}\Lambda\left(\Gamma_c + f\left(x, \Gamma_c\right)\right) \\ y &= Cx \end{aligned} \tag{43}$$

where C is a matrix capturing the the system output, $A \in \mathbb{R}^{nxn}$, $B \in \mathbb{R}^{nxm}$, and $C \in \mathbb{R}^{mxn}$ are known matrices. $\Lambda \in \mathbb{R}^{mxm}$ is an unknown but constant positive definite matrix, $x \in \mathbb{R}^n$ is the system state, $u \in \mathbb{R}^m$ is the control input, $y \in \mathbb{R}^m$ is the system output, and $f : \mathbb{R}^n \times \mathbb{R}^m \mapsto \mathbb{R}^m$ is Lipschitz continuous function that is unknown. The nominal vortex control law has the form

$$\Gamma_{C,n} = -K_y y + K_r r \tag{44}$$

where $K_y \in \mathbb{R}^{mxm}$ and $K_r \in \mathbb{R}^{mxr}$ where chosen such that the following reference system achieves the desired tracking characteristics

$$\begin{aligned} \dot{x}_m(t) &= A_m x_m(t) + B_m r \\ y_m(t) &= C x_m(t) \end{aligned} \tag{45}$$

where $A_m = A - BK_r$ is Hurwitz and $B_m = BK_r$. For the purposes of adaptive design, assume that A_m satisfies the following Lyapunov equation

$$A_m^T P + P A_m = -Q, \quad Q = Q^T > 0, \quad Q \in \mathbb{R}^{nxn} \tag{46}$$

To introduce an adaptive signal to compensate for $f(x, \Gamma_c)$, we redefine the total control effort as

$$\Gamma_C(t) = \Gamma_{C,n}(t) - \Gamma_{C,ad}(t) \tag{47}$$

Inserting the control law given in (42) into the open loop dynamics (43) the closed loop dynamics can be written

$$\begin{aligned} \begin{bmatrix} \dot{e} \\ \dot{x} \end{bmatrix} &= \begin{bmatrix} 0 & C \\ -\bar{B}K_I & \bar{A} - \bar{B}K_X \end{bmatrix} \begin{bmatrix} e \\ x \end{bmatrix} + \begin{bmatrix} -1 \\ \bar{B}Z \end{bmatrix} r + \begin{bmatrix} 0 \\ \bar{B} \end{bmatrix} \left(-u_{ad} + \Delta(x, x_a, \Gamma_c)\right) \\ \dot{x_a} &= g(x, x_a, \Gamma_c) \\ y &= \begin{bmatrix} 0 & C \end{bmatrix} \begin{bmatrix} e \\ x \end{bmatrix} \end{aligned} \tag{48}$$

One can rewrite the closed loop system in a more compact form as

$$\dot{x}(t) = A_m x(t) + B_m r + B\left[\delta\Lambda\Gamma_C(t) + \Lambda f(x, \Gamma_C) - \Gamma_{C,ad}\right] \tag{49}$$

We wish to approximate $\Lambda f(x, \Gamma_C)$ by a nonlinear in parameters neural network. To construct such an approximation in an output feedback setting[18–22] , we reconstruct the system states via delayed values of system outputs and inputs. If the number of delayed values for each output is s, the number of delayed values for each input is t, and the length of the time delay time is d, the delayed value vector, $\eta(t)$, is given by

$$\begin{aligned} \eta(t) = [[&y_1(t), y_1(t-d), ..., y_1(t-sd), ..., y_m(t), y_m(t-d), ..., y_m(t-sd)]^T; \\ &[\Gamma_{C,1}(t-d), ..., \Gamma_{C,1}(t-sd), ..., \Gamma C, m(t-d), ..., \Gamma_{C,m}(t-sd)]^T] \end{aligned} \tag{50}$$

where $\eta(t) \in \mathbb{R}^w$ and $w = (s+t)m$. Note that the current control output is not included in $\eta(t)$. This is prevent to implementation issues associated with realizing the control. Using $\eta(t)$, we assume that the function $f(x, \Gamma_C)$ can be approximated over a compact set $\mathcal{D}_x \times \mathcal{D}_{\Gamma_C}$ to an arbitrary degree of accuracy such that

$$\Lambda f(x, \Gamma_C) = W^T \bar{\sigma}(V^T \eta(t)) + \epsilon(x, \Gamma_C), \quad (x, \Gamma_C) \in \mathcal{D}_x \times \mathcal{D}_{\Gamma_C} \tag{51}$$

where $\|\epsilon(x, \Gamma_C)\| < \epsilon^* < \infty$, $\bar{\sigma}(q) = [1, \ \sigma_1(q_1), \ \cdots, \sigma_1(q_l)]$, l is the number of hidden layer neurons, $\sigma_i(z) = \frac{1}{1+exp(-z)}$ and $W \in \mathbb{R}^{(l+1)xm}$ and $V \in \mathbb{R}^{wxl}$ are unknown but constant neural network ideal weights. The closed loop system can then be equivalently expressed as

$$\dot{x}(t) = A_m x(t) + B_m r + B\left[\delta\Lambda\Gamma_C(t) + W^T \bar{\sigma}(V^T \eta(t)) - \Gamma_{C,ad}\right] + B\epsilon(x, \Gamma_C) \tag{52}$$

To develop the complete output feedback algorithm, an error observer must be introduced. Consider the following error observer

$$\begin{aligned} \dot{\xi} &= A_m \xi + L(y - y_\xi - y_m) \\ y_\xi &= C\xi \end{aligned} \tag{53}$$

such that $\tilde{A} = A_m - LC$ is Hurwitz and satisfies the following Lyapunov equation

$$\tilde{A}^T \tilde{P} + \tilde{P}\tilde{A} = -\tilde{Q}, \quad \tilde{Q} = \tilde{Q}^T > 0, \quad \tilde{Q} \in \mathbb{R}^{nxn} \tag{54}$$

The adaptive control signal is given as

$$u_{ad} = \left[I_m + \hat{\delta\Lambda}\right]^{-1} \left[\hat{\delta\Lambda} u_n + \hat{W}^T \bar{\sigma}\left(\hat{V}^T \eta(t)\right)\right] \tag{55}$$

The adaptive update laws are defined as

$$\begin{aligned} \dot{\hat{W}}(t) &= -\Gamma_W Proj\left[\hat{W}(t), \tilde{\sigma}\left(\hat{V}(t), \eta(t)\right) \xi(t)^T PB\right] \\ \dot{\hat{V}}(t) &= -\Gamma_V Proj\left[\hat{V}(t), \eta(t)\xi^T PBH\left(\hat{W}(t), \hat{V}(t), \eta(t)\right)\right] \\ \dot{\hat{\delta\Lambda}}^T(t) &= -\Gamma_\delta Proj\left[\hat{\delta\Lambda}^T(t), u(t)\xi^T(t)PB\right] \end{aligned} \tag{56}$$

where

$$\begin{aligned} \tilde{\sigma}\left(\hat{V}(t), \eta(t)\right) &= \bar{\sigma}\left(\hat{V}(t)^T \eta(t)\right) - \bar{\sigma}'\left(\hat{V}(t), \eta(t)\right) \hat{V}^T(t)\eta(t) \\ H\left(\hat{W}(t), \hat{V}(t), \eta(t)\right) &= \hat{W}^T(t)\bar{\sigma}'\left(\hat{V}(t), \eta(t)\right) \end{aligned} \tag{57}$$

and

$$\bar{\sigma}'\left(\hat{V}(t), \eta(t)\right) = \begin{bmatrix} 0 & \cdots & 0 \\ \frac{d\sigma_1(dq_1(t))}{dq} & \cdots & 0 \\ \vdots & \ddots & \vdots \\ 0 & \cdots & \frac{d\sigma_l(dq_l(t))}{dq} \end{bmatrix} \tag{58}$$

where q_i is the i^{th} row of $q = \hat{V}(t)^T \eta(t)$. Its easy to show with a standard Lyapunov candidate that the adaptive weights are bounded and that the system tracking error is uniformly ultimately bounded.

The modeling error $f(x, \Gamma_c)$ is a function of unmodeled flow dynamics as well. In the absence of an analytical model for flow actuation dynamics and devices to measure the related states, we can only use measurable states in the adaptive controller. In the relatively low bandwidth maneuvers performed in our experiments, the effects of flow dynamics on rigid body dynamics are expected to be small. In addition, we also assume that such effects are observable from rigid body states. With these assumptions, the adaptive signal defined in 55 can be used to approximate $f(x, \Gamma_c)$.

V.B. Control Hedging

In order to prevent adaptation to effects due to control saturation control hedging has been applied to modify the reference model (45). The difference between the commanded control and the control applied to the plant is defined as the hedge signal. The hedge signal is then subtracted from the input to the plant model of the reference model as shown in figure V.B. This modification effectively moves the reference model backwards by an estimate of the amount the controlled system did not move due to saturation and produces a reachable command within the capabilities of actuation. With this modification during periods of full saturation tracking error remains small, preventing winding up of the NN weights.

Applying control hedging to the adaptive vortex control algorithm in this paper requires the hedging algorithm to be gain scheduled. The reference model is modified as

$$\dot{x}_m = A_m x_m + B_m r + B_h \Gamma_{C,h}$$

where B_h is the modeled control effectiveness matrix. The hedge signal is computed as

$$\Gamma_{C,h} = g(u_f, \theta) - \Gamma_C$$

where $g(u_f, \theta)$ models the saturation limits of the actuator and Γ_C is the ideal control action. This is illustrated graphically in figure V.B and the actuator model, $g(u_f, \theta)$ is shown in figure V.B.

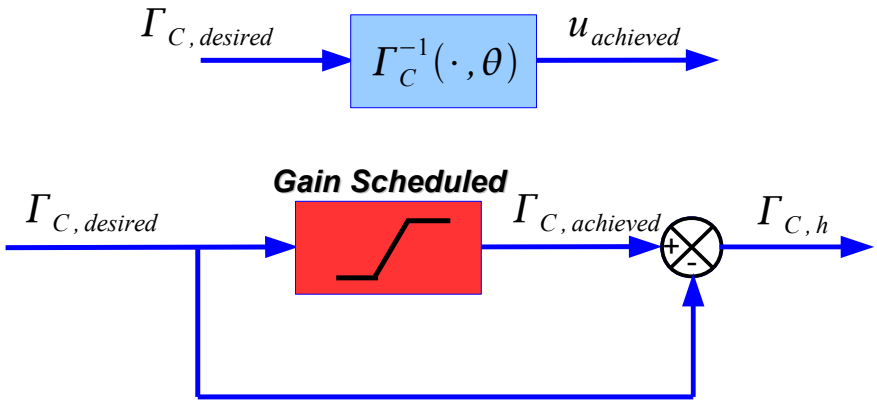

Figure 6. Control Hedging diagram.

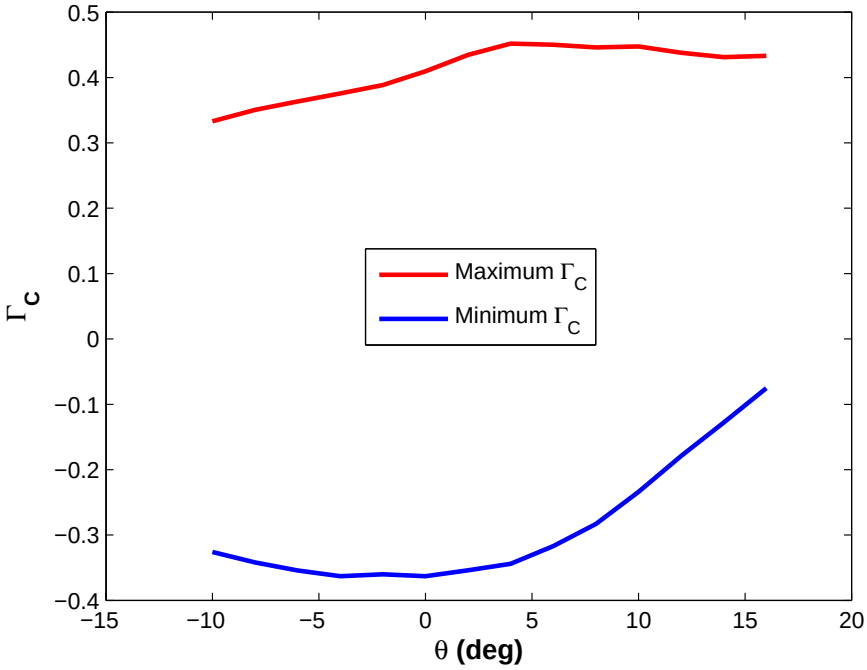

Figure 7. Gain scheduled saturation block.

VI. Model and Control Design Validation

Experimental verification of the model was performed under open loop excitation.[9] Numerical simulations were also used to validate the models in situations not realizable by the experiments. The numerical

simulations were computed at the University of Texas at Austin using a Delayed Detached Eddy Simulation (DDES). The DDES scheme is a hybrid non-zonal Reynolds-Averaged Navier-Stokes (RANS) and Large-Eddy Simulation (LES) turbulence model based on the Detached Eddy Simulation (DES) model. Simulations were run at a free-stream Reynolds number, $Re = 9 \times 10^5$. In this section, the model developed in our previous research was used to validate control design effort under high bandwidth free flight conditions and wind tunnel experiments conducted on a novel traverse capable of simulating free flight was used to further validate the control algorithms.

VI.A. Experimental Determination of Control Vortex Strength vs. Actuator Input Voltage

In the development of the control law, the control input was assumed to be Γ_c. In reality, a control moment is generated via a continuous signal (DC voltage) representing a commanded change amplitude modulation. The effect is analogous to a commanded control surface deflection in conventional flight control. Positive control signal indicates nose up moment and requires activation of the pressure side (PS) actuators and similarly negative control signal requires activation of the suction side (SS) actuators. Alternate amplitude-modulated operation of SS (top) and PS (bottom) actuators with a sample control signal is shown in figure 8.

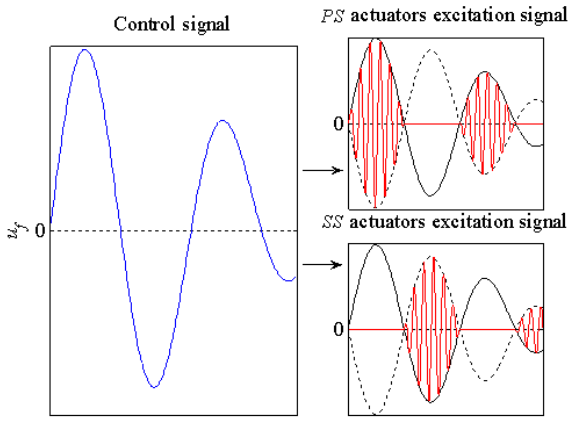

Figure 8. Amplitude Modulated Flow Actuation

It has been previously shown that the usage of synthetic jets traps vorticity in the boundary layer to directly modify the flow in the average sense.[4,23] This can be also be viewed as "virtual shaping" of the airfoil since this modifies the streamlines in the vicinity of the actuator. Here we model this "virtual shaping" or trapped vorticity as a stationary control vortex that depends on the control parameter (e.g. voltage), u. Since the PS and SS actuation do not act at the same time, the control vortex can be thought of as one vortex (situated on the x-axis) with a positive strength representing PS actuation and a negative strength representing SS actuation. Experiments show that the pressure distribution away from the neighborhood of the actuation point is essentially unaffected. This leads to the conclusion that no net circulation is injected into the wake as a direct consequence of turning the actuation on or off.

For simplicity, we model the actuation with a single vortex located on the x-axis. If the time scale for formation of $\Gamma_C << c/U$ then it can be assumed that the control vortex depends on only the control input, u, and the angle of attack, θ, such that

$$\Gamma_C = g(u_f, \theta). \tag{59}$$

This is sufficient for the situations where the time-scale for the formation of the vortex is much smaller than the convective time-scale, a more rigorous method of identification of a function in the form of Eq. 2) may be required for other cases. Given this assumption, one can generate a lookup table (or approximate function) for Γ_C based on steady state information. If there are no dynamics in the system we find

$$C_M(u, \theta) = \frac{\pi\theta}{2}\left(1 - \frac{4a}{c}\right) - \frac{2\Gamma_C}{Uc^2}\left(a + \xi_C\right). \tag{60}$$

Subtracting the moment at $u = 0$ we obtain

$$\Delta C_M(u,\theta) = C_M - C_{M,u=0} = -\frac{2\Gamma_C}{Uc^2}\left(a + \xi_C\right). \tag{61}$$

Now an equation for Γ_C given the distance ξ_C (e.g. $\xi_C = 0.45c$) is given by

$$\frac{\Gamma_C}{Uc} = -\frac{1}{2}\left(\frac{a}{c} + \frac{\xi_C}{c}\right)^{-1} \Delta C_M. \tag{62}$$

Thus we conduct the following: we span the space of $u \in [-u_{min}, u_{max}]$ and $\theta \in [\theta_{min}, \theta_{max}]$ and calculate the steady moment (after transients have been removed), C_M. Next, Eq. (62) is used to generate a look up table, i.e. interpolation is used to find the value of Γ_C given u and θ. Plotted in figure 9 is the approximate function corresponding to Eq. (62). Notice that the function is nearly independent of angle of attack as expected. The trapped vorticity should not depend strongly on angle of attack but instead should depend strongly on the voltage supplied to the actuators.

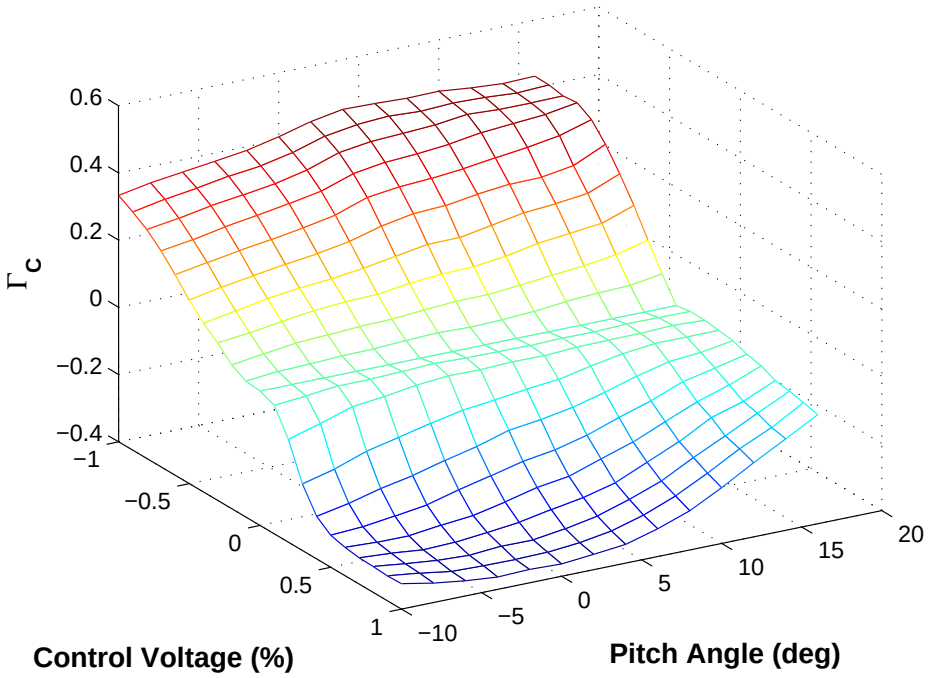

Figure 9. Experimental Approximation to $\Gamma_C(u_f, \theta)$

VI.B. Comparison Between Simulation Models and Experiment

In order to validate the static actuator model, linear vortex model and the non-linear vortex model, simulations using single degree of freedom model ($z = 0$ and $\dot{z} = 0$) were carried out and their results compared with experimental results. The experimental results were obtained with the ball screws locked in position so that the wing model was only allowed to pitch. The airfoil was then trimmed at an angle of attack, α, of 3 degrees with the torque motor providing the required torque. Then a series of doublets with an amplitude of 10 Volts and different durations were applied to the flow actuator in open loop as shown in Figure 10. The corresponding pitch response of the experiment was then compared with the simulations. As observed from the plots in Figure 11, the static actuator model response in pitch angle deviates significantly from the experimental response. This justifies our assumption that the static actuator model does not adequately capture the response of the flow actuator. As also observed from Figure 11, the linear vortex model and the nonlinear vortex model responses track the experimental results better than the static actuator model. Another interesting observation is that the response of the linear vortex model and the nonlinear vortex

model are almost equal and justifies the use of the linear vortex model for control design instead of the nonlinear vortex model.

VI.C. Regulating Control Vortex Strength

The relationship between Γ_c and the input control voltage was assumed to be of the form $\Gamma_c = g(u, \theta)$. This results in a system model of the form

$$\dot{\bar{x}} = \bar{A}\bar{x} + \bar{B}g(u, \theta) \tag{63}$$

For control, if $\Gamma_C(\cdot, \cdot)$ was invertible in u, the system could be inverted. Clearly form figure 9, for a given θ, the mapping $\Gamma_C(\cdot, \cdot)$ is really invertible. Examining figure 12, which plots Γ_C vs. u for fixed θ, we see that the effect of the input control voltage effectively can saturate in two ways. The total control voltage can saturate and the magnitude of Γ_C can saturate. When the input voltage increases above a point, Γ_C no longer increases in magnitude (it indicates control reversal). If we restrict the control, the curve for fixed θ is monotonic on a compact set which implies invertibility over the restricted domain. We also see that depending on θ, the maximum and minimum Γ_C shrinks in magnitude. Therefore, we have an angle of attack saturation dependence. We can use this information to develop the following feedback linearization strategy.

- Use control law formulation to compute required Γ_C
- Use interpolation over θ to determine $[max\ \Gamma_C, min\ \Gamma_C]$. Determine if Γ_C is achievable.
  - If Γ_C is achievable, compute corresponding control voltage.
  - If Γ_C is not achievable, apply the *best* control voltage possible and the appropriate control hedge signal.

This strategy can be realized in a lookup table and precomputed. This precomputed lookup table is shown in figure 12. In this figure, the inverse map is saturated. Note that since Γ_c is a continuous signal, the corresponding control voltage will also be continuous.

VI.D. Experimental Results

The control strategy for the experiments is as follows. First, the traverse is operated in position control mode where a tracking control design is used to drive the model to a desired position and attitude. Then position control is transferred to the flow actuator loop while the traverse is switched to the force control mode. In this mode, the traverse maintains the forcing derived from the required system dynamic properties while the outer loop controller, based on the control laws described previously, forces the modified dynamics of the wing model to track the given reference trajectory. In this paper, a variable force is applied to the model via the force control law to remove *only* the effect of gravity and friction. The outer loop control design assumes that ideal force tracking is achieved in the plunge axis and makes no account for the presence of the traverse. This assumption has proved sufficient.[24] It is also assumed that rigid body state information is available; consisting of vertical position, pitch attitude, and their derivatives. State estimation is achieved using a Kalman filter to blend sensed angular position and angular acceleration in the pitch axis, and by differentiation of sensed vertical positions in plunge. The flow state is unknown in all designs.

VI.D.1. Simulating Free Flight

Force control is a technique commonly used in robotics to control the position of a manipulator and its applied force. Here we control the forces and moments that are applied to a wind tunnel model in order to simulate the complete longitudinal dynamics of an arbitrary aircraft configuration. The techniques used in this application are different than those used in robotics because the force must be applied on a system while in motion and the control system must restrict the model to stay in the longitudinal plane regardless of the commanded and applied disturbance forces on the plunge axis. The control objective is achieved by manipulating the forces applied by two servo driven ball screws and the moment applied by a servo motor in the pitch axis. Applying a prescribed force to the model is difficult due to the large mass and high friction of the linear drives in relation to the model. The limitations in force control arise from the lack of compliance

between the model and the linear actuator. Having a stiff coupling between the actuator and the point of force application can cause a chattering effect. This is due to a large stiffness at the force measurement point. Furthermore, a stiff coupling results in poor force tracking. This is due to the actuators not being able to respond quickly enough to maintain an acceptable level in force tracking error. To overcome these limitations, linearly compliant springs were mounted between the model and each ball screw carriage as shown in figure 13. The contact force between the actuator and the model can then be precisely regulated through control of the spring deflections.

In order to study aircraft flight in a wind tunnel on a traverse heavy enough to carry all of the support and measurement equipment, the control system must serve three fundamental purposes: removing the effect of the high traverse mass, modifying the stability characteristics of the model, and restricting the motion of the traverse to the longitudinal plane. To meet these requirements, a three loop control architecture was used that consists of the carriage control loop, the force control loop, and the stability modification loop. A distinguishing feature of the latter loop is the ability to actively compensate for the effect of the center of gravity offset from the model pivot. A full description on the force tracking control law used in this paper is described in Muse.[24]

VI.D.2. Experimental Results

In this section we present typical results from application of the control designs described previously. All linear control designs were tuned to have a theoretical response that is similar in behavior. We fixed the overshoot and required the response the have the same shape. To evaluate improvements in performance, we slowly increased the response rise time until each model failed. Each model was tuned based solely on the linear design model. No tuning was used. Figure 14 illustrates the behavior of the static model using a torque motor to simulate the assumed response of the actuators. The torque motor output was scaled to have the same control effectiveness as the measured actuator gain. The same control gains and were used to control the model. As seen in the figure the response closely matches the expected ideal response. Hence, the traverse is functioning as expected. Figure 15 compares the response of the vortex model based linear control design to a control design using the static model for a rise time of 0.39 seconds (rise time is defined as 10 percent to 90 percent os the final command). The gains for the static model based control law are the same ones used for the torque motor in figure 14. The linear control law in this case exhibits a limit cycle type behavior that does not decay. However, the vortex model response remains quite close to the ideal response. In figure 16, the bandwidth of the nominal vortex control law is increased further, in this case the system rise time is 0.19 sec. The vortex model seems to be stable but suddenly looses stability. However, the adaptive control law is able to maintain stable ideal tracking. Figure 17 gives a visual comparison between the responses of the each design at the limit of each model's closed loop performance.

VII. Conclusion

A novel low-order model was developed to facilitate flight control design using synthetic jets. To the authors knowledge, this is the first model developed for control design that is based solely on first principles based modeling. Though the model used for a linear control design helps achieve higher control bandwidths than achievable with a conventional modeling assumptions, as the control bandwidth is increases, the nonlinearities in the flow become large requiring adaptive control methods to maintain tracking performance and stability. The adaptive architecture uses a single hidden layer neural network with delayed system output and control values to observe and compensate for the unmodeled system dynamics and nonlinearities. Control designs were verified on a novel wind tunnel traverse capable of simulating free flight in a wind tunnel.

Acknowledgments

This work has been supported by AFOSR. The authors would also like to Dr. Ari Glezer of the Mechanical Engineering Department at Georgia Tech, and the members of his team (Dan Brzozowski and John Culp) for their efforts in making this research possible.

References

[1]Wu, J., Lu, X., Denny, A., Fan, M., and Wu, J., "Post-stall Flow Control on an Airfoil by Local Unsteady Forcing," *Journal of Fluid Mechanics*, Vol. 371, 1998, pp. 21–58.

[2]Petz, R. and Wolfgang, R., "Active Control of Seperation on Two and Three-Dimensional High Lift Configurations," *25th International Congress of the Aeronautical Sciences*, 2006.

[3]Smith, B. and Glezer, A., "The formation and evolution of synthetic jets," *Physics of Fluids*, Vol. 10, No. 9, 1998, pp. 2281–2297.

[4]Glezer, A. and Amitay, M., "Synthetic Jets," *Annual Review of Fluid Mechanics*, Vol. 34, 2002, pp. 1–36.

[5]DeSalvo, M. and Glezer, A., "Aerodynamic Performance Modification at Low Angles of Attack by Trailing Edge Vortices," *AIAA Proceedings*, No. 2004-2118, 2004.

[6]Kutay, A., Calise, A., and Muse, J., "A 1-DOF Wind Tunnel Experiment in Adaptive Flow Control," *AIAA Guidance, Navigation, and Control Conference*, 2006.

[7]Muse, J. A., Kutay, A. T., Brzozowski, D. P., Culp, J. R., Calise, A. J., and Glezer, A., "Dynamics Flight Maneuvering Using Trapped Vorticity Flow Control," *AIAA Aerospace Sciences Meeting*, January 2008.

[8]Muse, J. A., Kutay, A. T., and Calise", A. J., "Closed Loop Flow Control Using An Augmenting Error Minimization Adaptive Law," *AIAA Guidance, Navigation and Control Conference and Exhibit*, August 2008.

[9]Tchieu, A., Kutay, A., Muse, J., Calise, A., and Leonard, A., "Validation of a Low-Order Model for Closed-Loop Flow Control Enable Flight," *38th AIAA Fluid Dynamics Conference and Exhibit*, American Institute of Aeronautics and Astronautics, 1801 Alexander Bell Drive, Suite 500, Reston, VA, 20191-4344, USA, 2008.

[10]von Karman, T. and Sears, W., "Airfoil theory for non-uniform motion," *Journal of Aeronautical Sciences*, Vol. 5, 1938, pp. 379–390.

[11]Rott, N., "Diffraction of a weak shock with vortex generation," *Journal of Fluid Mechanics*, Vol. 1, 1956, pp. 111–128.

[12]Cheng, H., "Remarks on nonlinear lift and vortex separation," *Journal of Aeronautical Sciences*, Vol. 19, 1954, pp. 212–214.

[13]Brown, C. and Michael, W., "Effect of leading edge separation on the lift of a delta wing," *Journal of Aeronautical Sciences*, Vol. 21, 1954, pp. 690–694.

[14]Cortelezzi, L., *A theoretical and computational study on active wake control.*, Ph.D. thesis, California Institute of Technology, 1992.

[15]Naudascher, E. and Rockwell, D., *Flow-Induced Vibrations, An Engineering Guide*, A.A. Balkema Publishers, 1994.

[16]Abbott, I. and Deonhoff, A., *Theory of Wing Sections*, Dover Publications, Inc., 1959.

[17]AIAA Guidance, Navigation, and Control Conference, *A Trade Study On Missile Autopilot Design Using Optimal Control Theory*, 2007.

[18]Calise, A. J., Yang, B. J., and Craig, J. I., "Augmentation of an Existing Linear Controller with an Adaptive Element," Proceedings of the American Control Conference, May 2002.

[19]Yang, B. J., *Adaptive Output Feedback Control of Flexible Systems*, Ph.D. thesis, Georgia Institute of Technology, School of Aerospace Engineering, April 2004.

[20]Yang, B. J., Calise, A. J., and Craig, J. I., "Adaptive Output Feedback Control of a Flexible Base Manipulator," AIAA Guidance, Navigation, and Control Conference, Aug. 2004.

[21]Yang, B. J., Calise, A. J., and Craig, J. I., "Adaptive Output Feedback Control with Input Saturation," Proceedings of the American Control Conference, 2003.

[22]Volyanskyy, K. Y., Haddad, W. M., and Calise, A. J., "A new neuroadaptive control architecture for nonlinear uncertain dynamical systems: Beyond & and e-modifications," *Proc. 47th IEEE Conference on Decision and Control CDC 2008*, 9–11 Dec. 2008, pp. 80–85.

[23]Glezer, A., "Aspects of Low- and High-Frequency Actuation for Aerodynamic Flow Control," *AIAA Journal*, Vol. 43, No. 7, 2005, pp. 1501–1512.

[24]Muse, J. A. Kutay, A. T. and Calise, A. J., "Novel Force Control Traverse For Simulating UAV Flight In Wind Tunnel," *AIAA Atmospheric Flight Mechanics Conference and Exhibit*, August 2008.

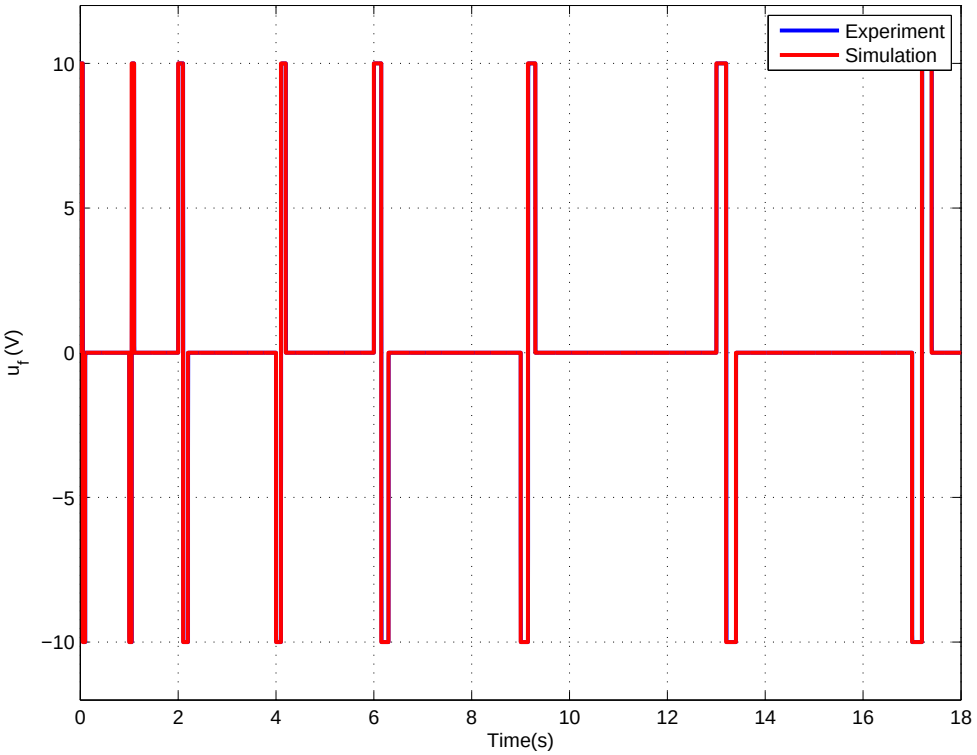

Figure 10. Pulse input applied to the flow actuator

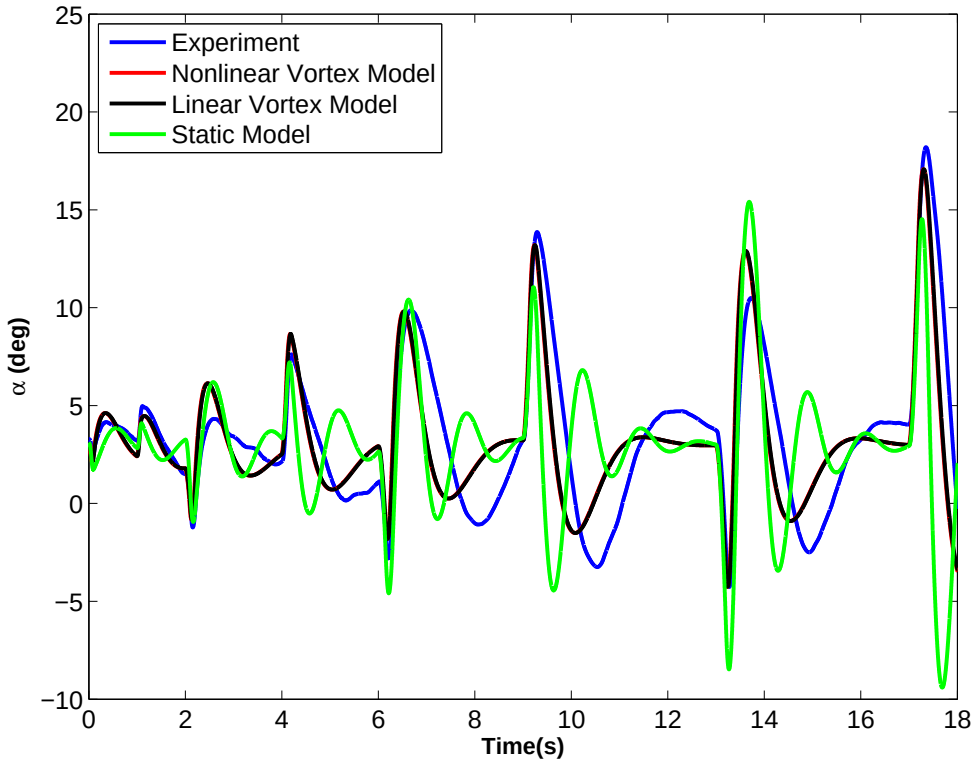

Figure 11. Pitch angle comparison of models with experimental data

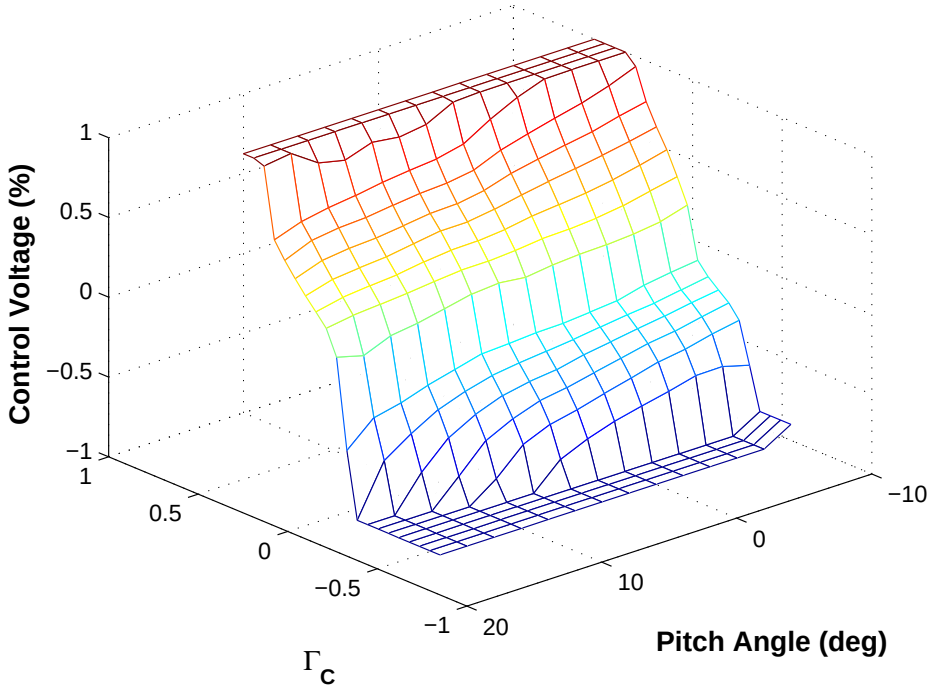

Figure 12. Γ_c^{-1} **with control voltage saturation limits**

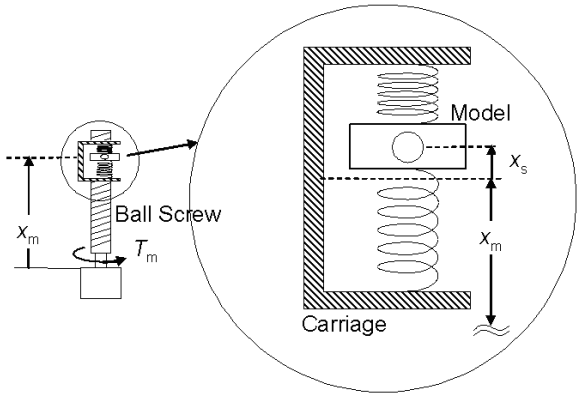

Figure 13. Diagram illustrating how the spring system interfaces to the wind tunnel model

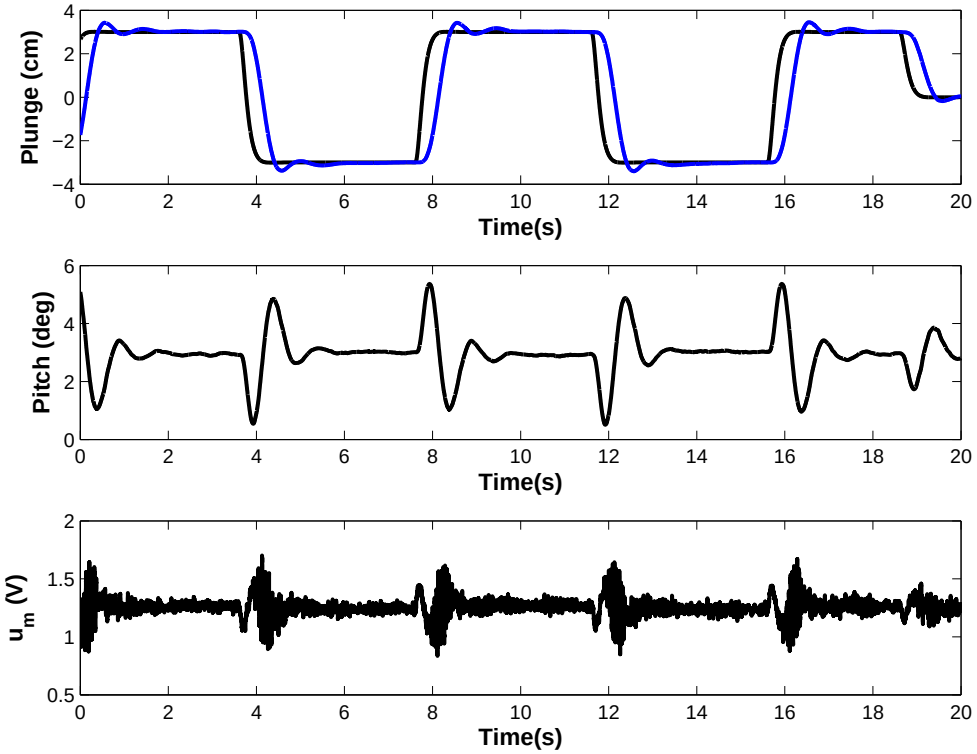

Figure 14. Verification that static model models response with torque motor accurately (Black - Command, Blue - Experimental Response).

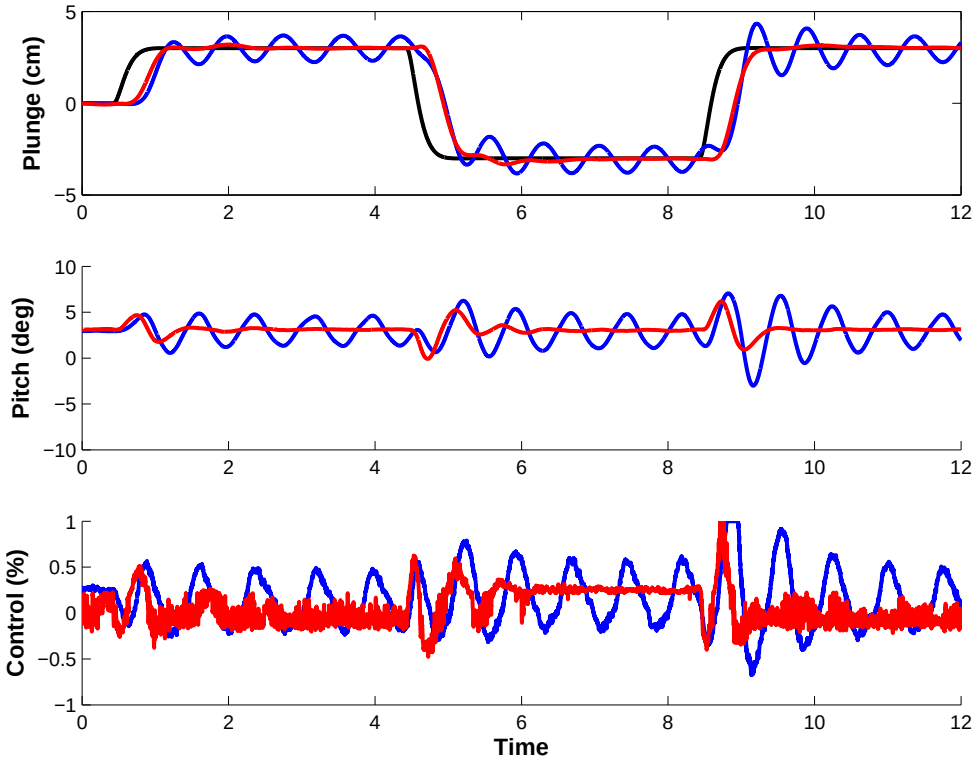

Figure 15. Comparison between vortex model and static model when static model assumption fails(Black - Command, Red - Vortex Model, Green - Adaptive Control Law).

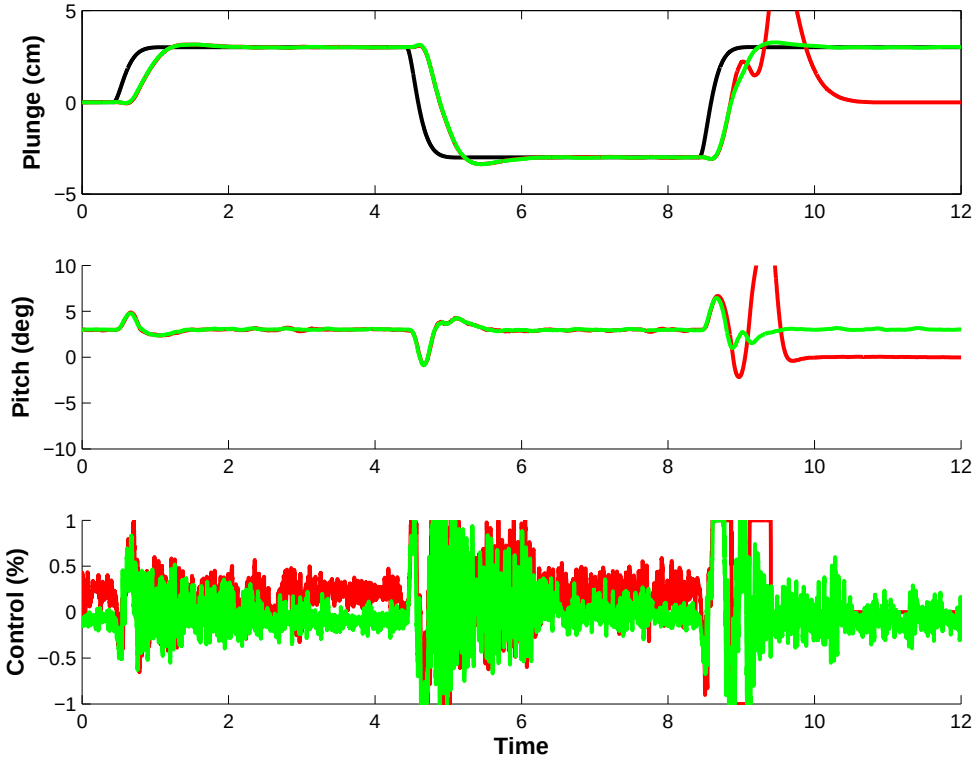

Figure 16. Comparison between vortex model and adaptive control law when vortex model fails.

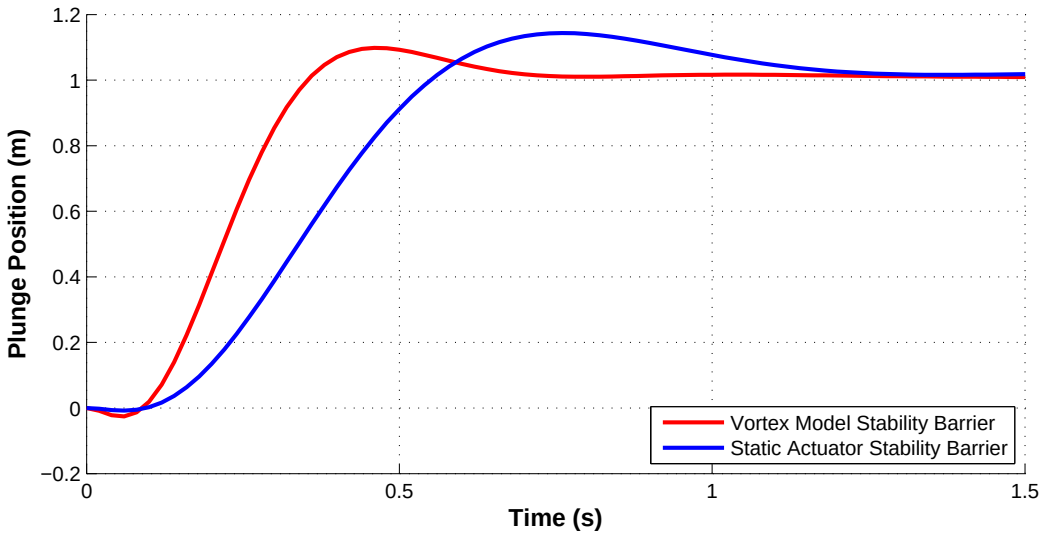

Figure 17. Comparison of rise time stability barriers.